

A Diruthenium Complex of a “Nindigo” Ligand

Prasenjit Mondal,[†] Fabian Ehret,[‡] Martina Bubrin,[‡] Amit Das,[†] Shaikh M. Mobin,[§] Wolfgang Kaim,^{*,‡} and Goutam Kumar Lahiri^{*,†}

[†]Department of Chemistry, Indian Institute of Technology Bombay, Powai, Mumbai 400076, India

[‡]Institut für Anorganische Chemie, Universität Stuttgart, Pfaffenwaldring 55, D-70550 Stuttgart, Germany

[§]Discipline of Chemistry, School of Basic Sciences, Indian Institute of Technology Indore, Indore 452017, India

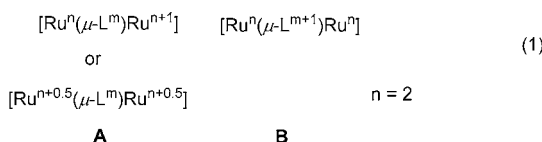
S Supporting Information

ABSTRACT: The compound $\{(\mu\text{-Nindigo})[\text{Ru}(\text{acac})_2]_2\} = \mathbf{1}$, H₂(Nindigo) = indigo-*N,N'*-diphenylimine and acac⁻ = 2,4-pentanedionate, has been structurally characterized in the *rac* form, which exhibits two edge-sharing six-membered chelate rings involving ruthenium, and the former β -diketiminato functions with a twist angle of 33.9° around the central C–C bond. The metric parameters suggest a neutral π acceptor bridge containing coupled *s-trans* configured α -diimines, which are coordinated by two ruthenium(II) centers. DFT calculations confirm the experimental structure and oxidation state assignment of the *rac* form; both diastereoisomers are present in solution according to ¹H NMR spectroscopy. A very intense long-wavelength MLCT absorption at 630 nm ($\epsilon = 66\,800\text{ M}^{-1}\text{ cm}^{-1}$) and a weaker near-IR band at 1120 nm ($\epsilon = 3000\text{ M}^{-1}\text{ cm}^{-1}$) are observed for the CH₃CN solution. Reversible one-electron reduction and oxidation steps were studied by cyclic voltammetry, differential pulse voltammetry, EPR, and UV–vis–NIR spectroelectrochemistry to exhibit metal-centered oxidation and mixed metal/ligand-centered reduction. These results are supported by TD-DFT calculations of the species *rac*- or *meso*-**1**ⁿ, $n = 3+, 2+, 0, -, 2-$.



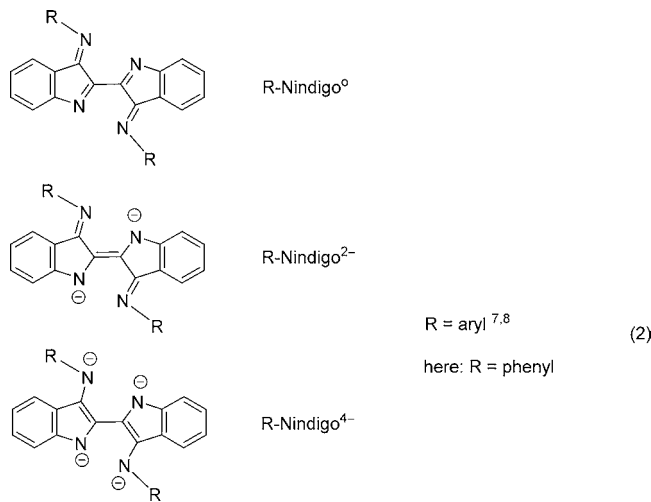
■ INTRODUCTION

Diruthenium complexes of redox-active and thus potentially noninnocently behaving bridging ligands have become rewarding subjects of electron transfer research¹ because they offer a readily analyzed alternative between a (Class II or Class III) mixed-valent metal–metal configuration with a super-exchanging bridge (A)² versus a homovalent dimetal arrangement with an oxidized radical bridge (B).³



Several different kinds of molecular bridges have thus been employed in connection with pairs of ruthenium complex fragments such as $[\text{Ru}(\text{bpy})_2]^{n+4}$ or $[\text{Ru}(\text{acac})_2]^{n+5}$. A recent addition to the set of bis-chelating unsaturated bridging ligands⁶ has been the $(\text{R-Nindigo})^n$ system (eq 2), $\text{H}_2(\text{R-Nindigo}) = \text{indigo-}N,N'\text{-diarylimine}$, derived from the indigo structure.⁷ Previous reports on some first coordination compounds containing Pd or Co have clearly suggested that the $(\text{R-Nindigo})^n$ systems can act as noninnocent ligands.^{7,8}

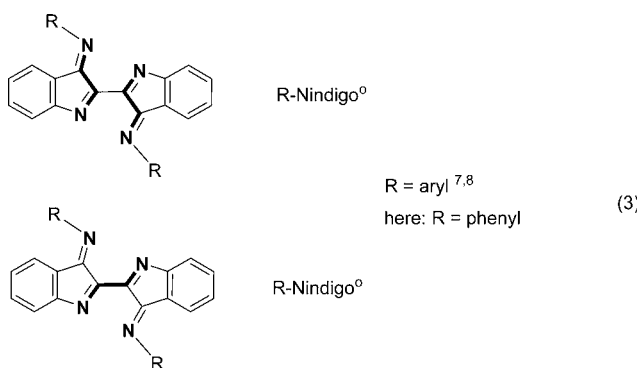
The Nindigo bridge is distinguished by being able to form dinuclear bis-chelate complexes with two fused six-membered chelate rings, in contrast to the better studied five-membered ring variety.^{4,5,9} In the neutral form, the two β -diketiminato functions sharing a common C–C edge also involve three *s-trans*-configured α -diimine sections (eq 3), another potentially redox-active moiety.¹⁰



According to eq 1, ruthenium is a prime candidate for studying metal/ligand electron transfer reactivity.^{2–6,11} Herein, we report a first study of a diruthenium complex, $\{(\mu\text{-Nindigo})[\text{Ru}(\text{acac})_2]\}_2 = \mathbf{1}$, $\text{H}_2(\text{Nindigo}) = \text{indigo-}N,N'$ -diphenylimine and $\text{acac}^- = 2,4\text{-pentanedionate}$, including the crystallographic characterization of $\mathbf{1}$ in the *rac* form, the spectroelectrochemical analysis of oxidation and reduction reactions of the *rac/meso* isomer mixture, and TD-DFT calculations of various species $\mathbf{1}^n$ in both *meso* and *rac* forms.

Received: February 14, 2013

Published: July 16, 2013



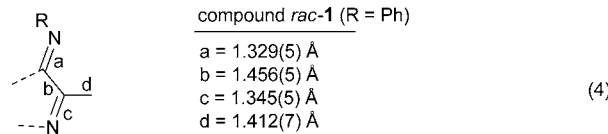
RESULTS AND DISCUSSION

Synthesis and Structure of 1. Reaction of H₂(Nindigo), NEt₃, and Ru(acac)₂(CH₃CN)₂ under atmospheric conditions in ethanol, followed by column chromatography, yields the product **1** in 60% yield. It was identified by CHN analysis, conductivity, mass spectroscopy and ¹H NMR spectroscopy (Experimental Section, Figures S1 and S4, Supporting Information) as a mixture of *meso* and *rac* diastereomeric forms due to the presence of two chiral metal centers; the single crystal isolated for X-ray diffraction was that of the *rac* isomer (Figure 1).

Aerial oxidation is assumed during the formation of **1** from reduced components, which is well-known to occur for dihydro compounds under basic conditions.¹² Side products accounting for 40% yield could not be removed from the column during chromatography. The use of dehydronindigo^{7a} gave essentially identical results.

The molecular structure of neutral **1** could be obtained for the *rac* form, which crystallized as a hydrate (Figure 1). Two C₂ symmetrical enantiomers and the water molecules are related by the inversion center in space group C₂/c. The molecular structure reveals a bis-chelate arrangement with two equivalent edge-sharing six-membered rings, each involving a chiral ruthenium center and one of the former β -diketiminato functions of (Nindigo)ⁿ. The oxidation state combination implying two Ru^{II} ions and an oxidized neutral ligand follows

from the metric parameters (eq 4, Table 1) of the bridging ligand,^{7,8} clearly corresponding to Nindigo⁰ ("dehydronindigo"^{7,8}) in eq 2.



Single and double bonds are well distinguished in the molecular structure and are incompatible with the charged forms of Nindigo in eq 2. Instead, they correspond to α -diimine structures in the *s-trans* conformation (eq 3). The central C–C bond at 1.412(7) Å separates two rings twisted by 33.9°, the previously reported central C–C bond lengths for coordination compounds of R-Nindigo ligands being slightly shorter at 1.396(15), 1.368(5), 1.379(7), or 1.393(2) Å.^{7a,b,8} The intramolecular metal–metal distance at 6.042 Å is longer than the approximately 4.8 Å found in compounds with edge-sharing five-membered chelate rings.^{5a} The N-phenyl rings are twisted relative to the C8–N2–C14 imine function with an angle of 83.4°. The structural features of this *rac* isomer of **1** could be reproduced by DFT calculations (Table 1 and Tables S1, S2, Figure S2, Supporting Information), including the central C–C twist angle of 30.6° (exp.: 33.9°). Because the studies in solution described in the following were carried out with a mixture of *rac* and *meso* forms, the latter has also been calculated by DFT to show only marginal differences relative to the *rac* isomer (e.g., 31.6° C–C twist angle; Tables S3, S4 and Figure S3, Supporting Information).

Spectroscopy. The observed diamagnetism of **1**, including conventional ¹H NMR resonances (Experimental Section and Figure S4, Supporting Information), is in agreement with two low-spin d⁶ centers bridged by a closed-shell ligand. The ¹H NMR spectrum of **1** in CDCl₃ exhibits eight CH₃(acac), four CH(acac), and 18 "aromatic" proton resonances (Experimental Section and Figure S4), corresponding to the presence of both *meso* and *rac* isomeric forms.

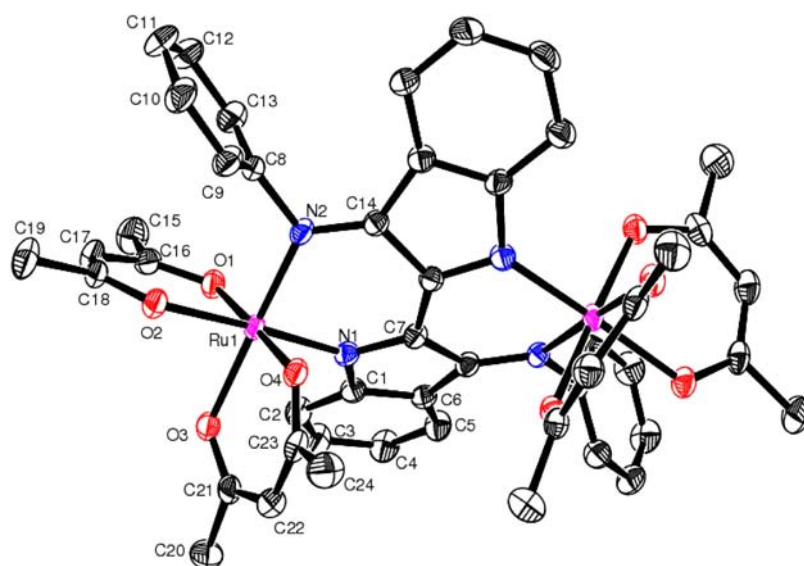


Figure 1. ORTEP diagram of the *rac*-form of **1**. Ellipsoids are drawn at the 50% probability level. Hydrogen atoms and solvent molecules are omitted for clarity.

Table 1. Experimental and DFT Calculated Selected Bond Distances (\AA) and Bond Angles (deg) in **1** (*rac*)

bond distance (\AA)	X-ray	DFT	bond angle (deg)	X-ray	DFT
Ru1–N2	1.976(3)	2.034	N2–Ru1–N1	90.04(12)	89.08
Ru1–N1	1.992(3)	2.040	N2–Ru1–O4	85.24(11)	84.75
Ru1–O4	2.016(3)	2.068	N1–Ru1–O4	90.85(11)	90.65
Ru1–O1	2.042(3)	2.086	N2–Ru1–O1	94.88(12)	96.15
Ru1–O3	2.043(3)	2.081	N1–Ru1–O1	91.01(12)	90.93
Ru1–O2	2.061(2)	2.098	O4–Ru1–O1	178.14(10)	178.18
N1–C7	1.345(5)	1.335	N2–Ru1–O3	177.14(11)	175.39
N2–C14	1.329(5)	1.313	N1–Ru1–O3	90.29(11)	93.26
C7–C7#1	1.412(7)	1.419	O4–Ru1–O3	91.92(10)	91.24
C14–C7#1	1.456(5)	1.476	O1–Ru1–O3	87.95(10)	87.78
Ru1–Ru1#1	6.042	6.092	N2–Ru1–O2	91.34(11)	92.88
			N1–Ru1–O2	176.65(11)	177.17
			O4–Ru1–O2	86.23(10)	87.51
			O1–Ru1–O2	91.91(11)	90.87
			O3–Ru1–O2	88.18(10)	84.63

Table 2. UV–Vis–NIR Spectroelectrochemical Data of **1ⁿ** in CH₃CN/0.1 M Bu₄NPF₆

	λ [nm] (ϵ [$M^{-1} \text{ cm}^{-1}$])
1ⁿ	720(34 610), 620(26 430), 580(25 190), 430(24 500), 270(63 100), 240(70 130), 210(80 510)
1³⁺	720(28 610), 620(30 730), 580(sh), 430(24 690), 340(31 660), 270(65 780), 240(66 410), 210(77 810)
1²⁺	1120(1520), 780(sh), 620(47 520), 500(sh), 340(37 700), 270(70 190), 210(76 400)
1⁺	1120(3000), 630(66 820), 520(sh), 360(39 120), 270(84 680), 210(69 650)
1	850(16 320), 590(27 160), 400(sh), 360(36 830), 270(95 140), 210(93 450)
1⁻	1120(10 150), 850(sh), 500(33 060), 380(sh), 280(110 880), 220(98 490)
1²⁻	

The typical intense absorption of the indigo chromophore in the visible occurs around 600–650 nm with $\epsilon \approx 15\,000 \text{ M}^{-1} \text{ cm}^{-1}$, attributable to an internal donor (amine-N)-to-acceptor (CO) transition. H₂(R-Nindigo) species have similar spectral features (amine-to-imine transition).^{7,13} In the present case **1**, the absorption of the metal complex is also observed at a wavelength of about 630 nm, however, with a significantly larger molar extinction coefficient of $\epsilon = 66\,800 \text{ M}^{-1} \text{ cm}^{-1}$ (see Figure 3a and Table 2). An additional weak, broad absorption occurs at 1120 nm ($\epsilon = 3000 \text{ M}^{-1} \text{ cm}^{-1}$). TD-DFT calculations (Table 3 (*rac*), Table S21 (*meso*), Supporting Information) were used to assign both of these features as MLCT (d→π*, metal-to-ligand charge transfer) transitions from electron-rich Ru^{II} to the neutral Nindigo⁰ acceptor, which features coupled *s-trans* configurated α-diimine functions (eq 3).¹⁰ Characteristically, the neutral form in eq 2 features quinonoid pyrrole rings, whereas both dianionic and tetraanionic charged forms contain 6π heteroaromatic pyrrole rings. Both the metal-originated multiple charge transfer and the quinonoid electronic structure are believed to contribute to the high intensity of the absorption of **1** in the visible region.

Electrochemistry and EPR. The potential of coordinated R-Nindigo species to act as noninnocent ligands^{7,8} with possible oxidation or reduction was probed for **1** by cyclic voltammetry, differential pulse voltammetry, EPR, and UV–vis–NIR spectroelectrochemistry. Figure 2 and Table 4 show that two one-electron reduction steps and three oxidation steps can be discerned. The third oxidation is less well-defined, and the comproportionation constants K_c ($RT \ln K_c = nF(\Delta E)$) for the monocation and monoanion are rather large at about 10¹⁰.

The DFT calculated molecular orbital compositions on optimized geometries of **1ⁿ** in both *meso* and *rac* forms (Tables S5–S18, Supporting Information) suggest the involvement of {Ru(acac)₂} fragment and mixed ligand(nindigo)-metal frontier

orbitals in the successive oxidation and reduction processes, respectively.

Electrogenerated **1⁺** and **1⁻** were analyzed by EPR spectroscopy (Figure 4). At 110 K in frozen acetonitrile solution, both systems exhibit rhombic spectra; however, with $g_1 = 2.334$, $g_2 = 2.180$, $g_3 = 1.831$, and $g_1-g_3 = 0.503$, the g factor anisotropy of **1⁺** is almost 5 times larger than for **1⁻** ($g_1-g_3 = 0.112$), corresponding clearly to metal-centered spin¹⁴ and thus to a Ru^{III}Ru^{II} mixed-valent situation with a (Nindigo)⁰ acceptor bridge. Remarkably, there is no conspicuous intervalence charge transfer (IVCT) absorption in the near-infrared region for **1⁺**, in agreement with the frequently noted low intensity of such π*-mediated IVCT absorptions in bischelate situations.^{6,15}

The reduction to **1⁻** produces a labile species with an EPR spectrum ($g_1 = 2.031$, $g_2 = 2.003$, $g_3 = 1.919$), the g anisotropy $g_1-g_3 = 0.112$ suggesting a mixed metal/ligand-centered spin distribution,^{14,16} corresponding to significant {Ru^{II}[$(\mu$ -Nindigo)^{•-}]Ru^{II}} and {Ru^{III}[$(\mu$ -Nindigo)²⁻]Ru^{II}} participation. DFT calculated spin densities (Figure 5, Table 5 for *rac* form, and Figure S5, Table S22 for *meso* isomer, Supporting Information) support and quantify this experimental result, yielding very different metal spin density values of 1.208 for **1⁺** but of 0.440 for **1⁻** in the *rac* form (*meso* form: 1.231 and 0.486 for **1⁺** and **1⁻**, respectively). Again, no significant near-IR absorption was observed.

UV–Vis–NIR Spectroelectrochemistry. Analysis of the full set of UV–vis–NIR spectroelectrochemical information (Figure 3, Table 2) requires an understanding of the underlying electronic structures based on DFT calculated geometries (Tables S1–S4, Supporting Information), molecular orbital situations (Tables S5–S20, Supporting Information), and electronic transitions (TD-DFT: Table 3 for *rac* and Table S21 for *meso*, Supporting Information).

Table 3. Experimental^a and TD-DFT (B3LYP/CPCM/CH₃CN) Calculated Electronic Transitions for **1ⁿ** (*rac*)

state	λ [nm]	expt. (DFT)	ε [$M^{-1} \text{ cm}^{-1}$] (f)	transitions	character
				1 ($S = 0$)	
2	1120 (1252)		3020 (0.03)	HOMO→LUMO(0.53)	Ru(d π)→L(π^*)
8	630 (623)		66 820 (0.23)	HOMO-1→LUMO+1(0.47)	Ru(d π)→L(π^*)
				HOMO-3→LUMO+1(0.34)	Ru(d π)→L(π^*)
				HOMO→LUMO(0.27)	Ru(d π)→L(π^*)
13	520 (512)		sh (0.07)	HOMO-8→LUMO(0.66)	acac(π)→L(π^*)
41	360 (361)		39 120 (0.02)	HOMO-11→LUMO+1(0.57)	L(π^*)→L(π^*)
72	270 (305)		84 680 (0.04)	HOMO-9→LUMO+1(0.30)	acac(π)→L(π^*)
				1⁺ ($S = 1/2$)	
5	1120 (1057)		1520 (0.02)	HOMO(α)→LUMO(α)(0.85)	acac(π)→L(π^*)
10	780 (758)		sh (0.08)	HOMO-2(α)→LUMO(α)(0.61)	acac(π)/Ru(d π)→L(π^*)
14	620 (646)		47 520 (0.10)	HOMO-7(β)→LUMO(β)(0.55)	acac(π)/Ru(d π)→Ru(d π)
33	500 (504)		sh (0.05)	HOMO-11(β)→LUMO(β)(0.55)	L(π)→Ru(d π)
				HOMO-8(β)→LUMO(β)(0.47)	L(π)→Ru(d π)
68	340 (400)		37 700 (0.04)	HOMO-7(α)→LUMO+1(α)(0.68)	L(π)→L(π^*)
				1²⁺ ($S = 1$)	
18	720 (721)		28 610 (0.07)	HOMO-2(α)→LUMO(α)(0.61)	acac(π)→L(π^*)
				HOMO-11(β)→LUMO(β)(0.33)	Ru(d π)/acac(π)→Ru(d π)/L(π^*)
27	620 (647)		30 730 (0.06)	HOMO-4(β)→LUMO+1(β)(0.44)	acac(π)→Ru(d π)
37	580 (572)		sh (0.04)	HOMO-12(α)→LUMO(α)(0.50)	Ru(d π)→L(π^*)
				HOMO-8(β)→LUMO+1(β)(0.57)	L(π)→Ru(d π)
70	430 (443)		24 690 (0.04)	HOMO-5(α)→LUMO+1(α)(0.40)	L(π)→L(π^*)
				HOMO-13(β)→LUMO+1(β)(0.66)	L(π)→Ru(d π)
				1³⁺ ($S = 1/2$)	
37	720 (700)		34 610 (0.12)	HOMO-14(α)→LUMO(α)(0.60)	L(π)/Ru(d π)→Ru(π^*)/acac(π^*)
				HOMO-6(β)→LUMO(β)(0.33)	acac(π)→Ru(d π)/acac(π^*)
				HOMO-4(β)→LUMO+1(β)(0.43)	L(π)→Ru(d π)/acac(π^*)
50	620 (628)		26 430 (0.06)	HOMO-3(α)→LUMO+1(α)(0.63)	L(π)→L(π^*)
69	580 (530)		25 190 (0.03)	HOMO-5(β)→LUMO+2(β)(0.26)	acac(π)→L(π^*)
80	430 (492)		24 500 (0.02)	HOMO-8(α)→LUMO+1(α)(0.65)	acac(π)→L(π^*)
				HOMO-13(α)→LUMO+1(α)(0.44)	L(π)→L(π^*)
				1⁻ ($S = 1/2$)	
9	850 (807)		16 320 (0.04)	HOMO-2(α)→LUMO(α)(0.52)	Ru(d π)→L(π^*)
				HOMO-4(β)→LUMO(β)(0.49)	Ru(d π)→L(π^*)
				HOMO-1(β)→LUMO+1(β)(0.45)	Ru(d π)→L(π^*)
14	590 (642)		27 160 (0.19)	HOMO-4(α)→LUMO(α)(0.46)	Ru(d π)→L(π^*)
				HOMO-1(β)→LUMO+1(β)(0.61)	Ru(d π)→L(π^*)
63	400 (395)		sh (0.03)	HOMO(α)→LUMO+8(α)(0.70)	L(π)→L(π^*)
77	360 (377)		36 830 (0.01)	HOMO-12(β)→LUMO(β)(0.32)	L(π)→L(π^*)
				1²⁻ ($S = 0$)	
3	850 (733)		sh (0.15)	HOMO-2→LUMO((0.60)	Ru(d π)→L(π^*)
18	500 (478)		33 060 (0.14)	HOMO-6→LUMO((0.60)	Ru(d π)→L(π^*)
38	380 (385)		sh (0.04)	HOMO-2→LUMO+5(0.40)	Ru(d π)→L(π^*)
				HOMO-3→LUMO+1(0.33)	Ru(d π)→acac(π^*)
72	280 (330)		110 880 (0.08)	HOMO-12→LUMO(0.63)	L(π)→L(π^*)
				1²⁻ ($S = 1$)	
3	850 (919)		sh (0.09)	HOMO-2(β)→LUMO(β)(0.90)	Ru(d π)→L(π^*)
				HOMO(β)→LUMO(β)(0.31)	Ru(d π)→L(π^*)
32	500 (497)		33 060 (0.05)	HOMO-6(β)→LUMO(β)(0.49)	L(π)→L(π^*)
				HOMO(β)→LUMO+4(β)(0.27)	Ru(d π)→acac(π^*)
80	380 (383)		sh (0.05)	SOMO(α)→LUMO-15(α)(0.74)	L(π)→Ru(d π)/acac(π^*)

^aExperimental data for *rac/meso* mixture.

From these and earlier discussed data, the following picture emerges, illustrated by Scheme 1.

Oxidation of the {Ru^{II}[(Nindigo)⁰]Ru^{II}} precursor **1** leaves the bridge unchanged and involves the metals and, for higher positive charges, the whole {Ru(acac)₂} metal complex fragments (Tables S5–S12, Supporting Information). The capacity of Ru(acac)₂ to get oxidized up to the formal Ru^{IV}

state under participation of the donating acac⁻ coligand is well established.¹⁷ Accordingly, the main long-wavelength absorptions of the cationic forms involve LMCT (ligand to metal charge transfer), LMLCT (ligand/metal to ligand charge transfer), and LLCT (ligand to ligand charge transfer) transitions (Table 3 for *rac* and Table S21 for *meso*, Supporting Information). The question of a localized or delocalized mixed-

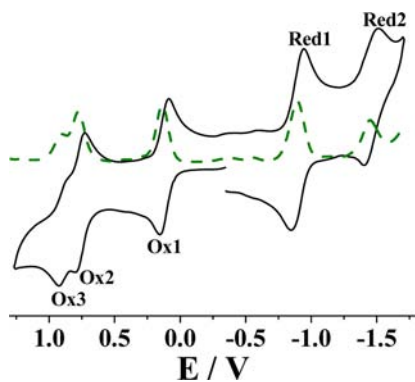


Figure 2. Cyclic voltammogram (—, black) and differential pulse voltammogram (---, green) of **1** in acetonitrile/NEt₄ClO₄ at 298 K. Scan rate: 100 mV s⁻¹.

valent intermediate **1**⁺ cannot be straightforwardly answered; the absence of an intense IVCT transitions seems to suggest weak electronic coupling (Class II according to Robin and Day¹⁸), while the large K_c value of 10¹¹ would be more compatible with a Class III (valence-delocalized) situation.

Reduction to **1**⁻ leads to the mentioned mixed metal/ligand formulation (Scheme 1) based on EPR (Figure 4) and spin density (Ru/Nindigo: 0.440/0.542 (*rac*) and 0.486/0.491

(*meso*)) information (Figure 5, Table 5 for *rac* and Figure S5, Table S22 for *meso*, Supporting Information). The calculated geometry of this ion would still be compatible with a neutral bridge (Tables S1–S4, Supporting Information), whereas the dianion, calculated with close lying singlet and triplet states (Tables S1, S20 for *rac* and S3, S19 for *meso*, Supporting Information), is computed with a lengthened N1–C7 bond (Tables S1 (*rac*), S3 (*meso*), Supporting Information), which indicates negatively charged pyrrole N atoms as in Nindigo²⁻ (eq 2). Low-energy absorptions of **1**⁰, **1**⁻, and **1**²⁻ are thus dominated by MLCT transitions (Table 3 (*rac*) and Table S21 (*meso*), Supporting Information).

CONCLUSION

In contrast to the previously reported palladium(II)^{7a,b} and cobalt(II)⁸ complexes, which illustrated the potential of R-Nindigo ligands to undergo up to four electron transfer steps and thus behave decidedly noninnocently, the present result involving the ruthenium complex fragments [Ru(acac)₂] revealed a less pronounced proclivity toward redox noninnocent behavior when compared to other ligand-bridged diruthenium complexes.^{4,5} Neutral and oxidized compounds **1**ⁿ ($n = 0, 1^0, 2^+, 3^+$) contain the bridge as dehydro-indigo-*N,N'*-diphenylimine, whereas the anionic species involve partially reduced Nindigo (Scheme 1). Remarkably, the MLCT

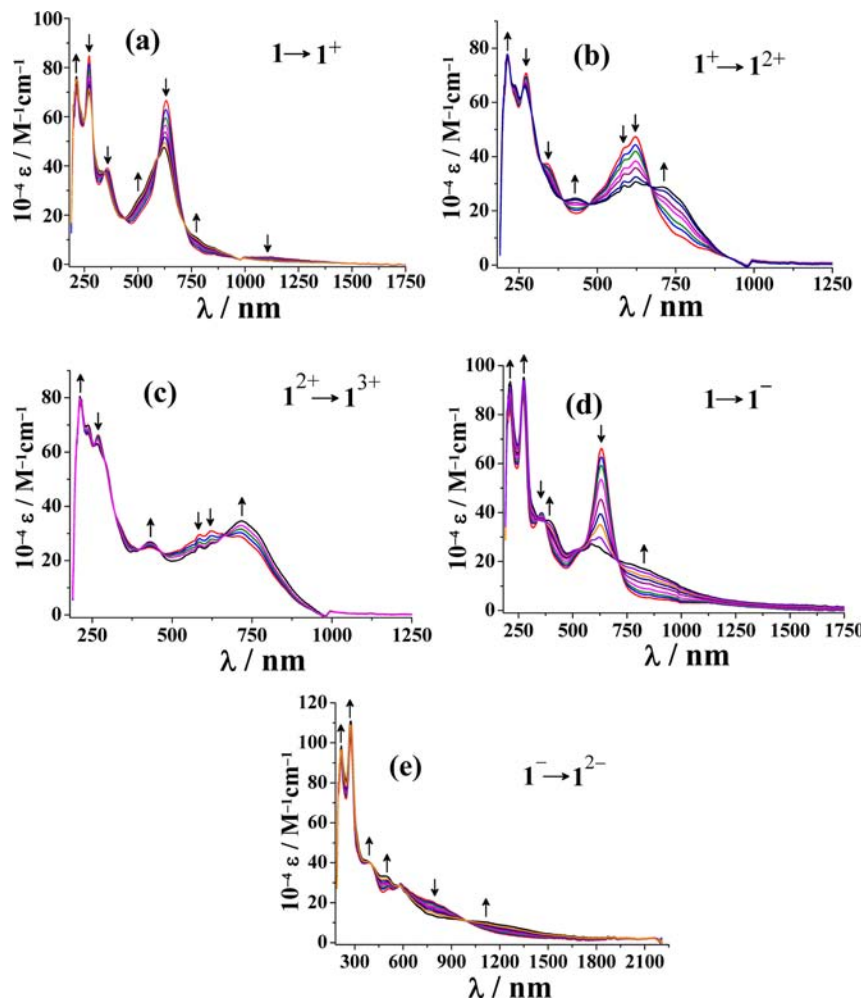
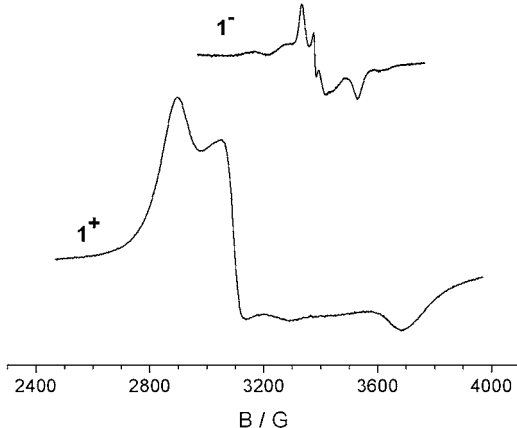


Figure 3. UV–vis–NIR spectroelectrochemistry for **1**ⁿ in CH₃CN/0.1 M NBu₄PF₆.

Table 4. Electrochemical Data^a for **1**

E°_{298} [V] (ΔE [mV]) ^b					$K_{c1}^{c,d}$	$K_{c2}^{c,e}$	$K_{c3}^{c,f}$	$K_{c4}^{c,g}$
Ox3 0.89 (50)	Ox2 0.76 (70)	Ox1 0.11 (70)	Red1 −0.88 (90)	Red2 −1.45 (110)	1.1×10^{11}	1.6×10^2	6.0×10^{16}	4.6×10^9

^aFrom cyclic voltammetry in $\text{CH}_3\text{CN}/0.1$ M Et_4NClO_4 at 100 mV s^{−1}. ^bPotential in V versus SCE; peak potential differences ΔE [mV] (in parentheses). ^cComproportionation constant from $RT \ln K_c = nF(\Delta E)$. ^d K_{c1} between Ox1 and Ox2. ^e K_{c2} between Ox2 and Ox3. ^f K_{c3} between Ox1 and Red1. ^g K_{c4} between Red1 and Red2.

Figure 4. EPR spectra of **1**[−] and **1**⁺ in $\text{CH}_3\text{CN}/0.1$ M NBu_4PF_6 at 110 K (shoulder at $g \approx 2$ due to decomposition product).

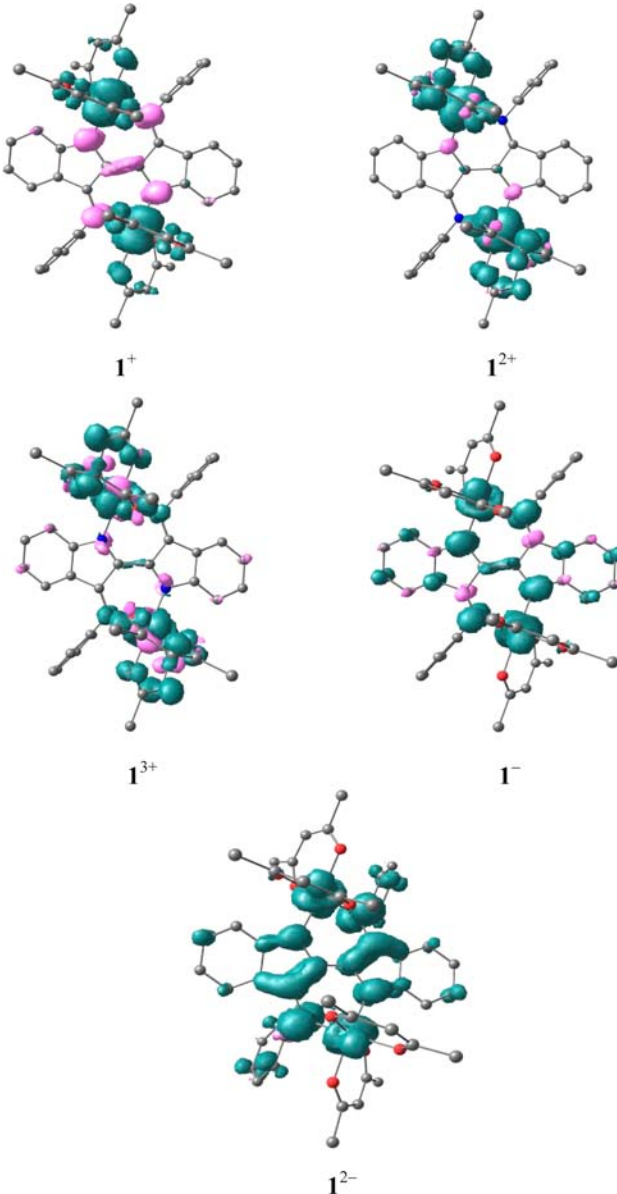
absorption of **1** occurring in the same spectral region (630 nm) as that of indigo exhibits a very high intensity at $\epsilon = 66\,800$ M^{−1} cm^{−1}. The fused double six-membered chelate ring arrangement in dinuclear coordination compounds of R-Nindigo ligands can thus be expected to produce further remarkable results with different metal species, considering the α -diimine substructures (eq 3) of the dehydro form.

The results from Scheme 1 based on experiments and calculations are surprising in that the $[\text{Ru}(\text{acac})_2]^{n+}$ complex fragment prefers higher oxidation states of the metal (+III, +IV), that is, $n = 1$ or 2.¹⁷ Examples include 2,2'-azobispyridine (abpy) and 1,4-dioxido-2,3-bis(3,5-dimethylpyrazol-1'-yl)-benzene (L^{2-}) bridged dinuclear complexes, which were isolated in forms describable as $[(\text{acac})_2\text{Ru}^{2.5}(\mu\text{-abpy}^\bullet)\text{Ru}^{2.5}(\text{acac})_2]$ ^{Se} and $[(\text{acac})_2\text{Ru}^{\text{III}}(\mu\text{-L}^{2-})\text{Ru}^{\text{III}}(\text{acac})_2]$ ^{Sd}, respectively. It is also unexpected that the R-Nindigo bridge adopts the twisted neutral dehydronindigo form instead of the 6π heteroaromatic dianionic form as preformed in the $\text{H}_2(\text{R-Nindigo})$ precursor. In the present situation, the twist is probably favored by the space demand of N-substituents and the $[\text{Ru}(\text{acac})_2]$ complex fragments; the dehydro form does not require planarity at the central C–C bond as does the dianion with a formal C=C double bond, which thus disfavors ligand-centered versus metal-based electron transfer.

EXPERIMENTAL SECTION

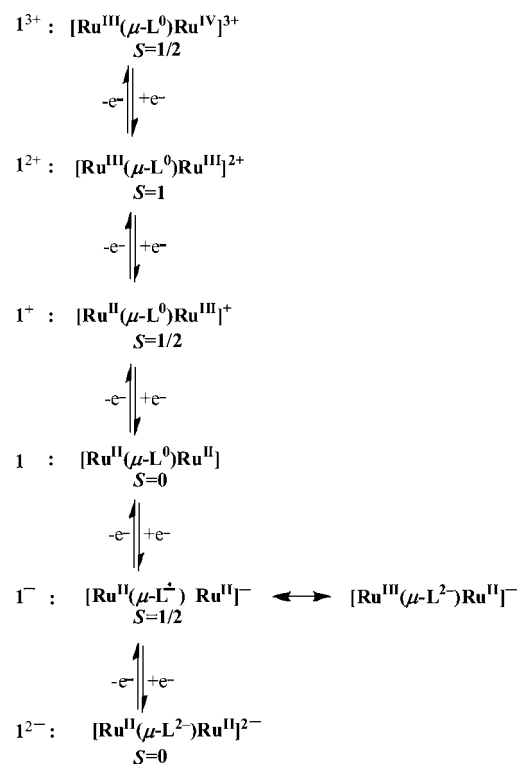
Materials. The starting complex, $[\text{Ru}(\text{acac})_2(\text{CH}_3\text{CN})_2]$,¹⁹ and the bridging ligand indigo-*N,N'*-diphenyldiimine^{7b} were prepared according to the literature reported procedures. Other chemicals and solvents were reagent grade and used without further purification. For spectroscopic and electrochemical studies, HPLC grade solvents were used.

Physical Measurements. UV-vis-NIR studies in $\text{CH}_3\text{CN}/0.1$ M Bu_4NPF_6 at 298 K were performed using an optically transparent thin layer electrode (OTTLE) cell,²⁰ which was mounted in the sample compartments of a J&M TIDAS spectrophotometer. ¹H NMR spectra were recorded on a Bruker Avance III 400 spectrometer. The EPR

Figure 5. DFT calculated Mulliken spin density plots of **1**ⁿ (*rac*).Table 5. DFT Calculated Mulliken Spin Distributions for **1**ⁿ (*rac*)

complexes	Ru	acac	L
1 ⁺ ($S = 1/2$)	1.208	0.148	−0.348
1 ²⁺ ($S = 1$)	1.482	0.599	−0.049
1 ³⁺ ($S = 1/2$)	0.506	0.498	0.003
1 [−] ($S = 1/2$)	0.440	0.020	0.542
1 ²⁻ ($S = 1$)	0.464	0.01	1.53

Scheme 1. Oxidation State Combinations for Different Redox States



measurements were made in a two-electrode capillary tube^{16a} with an X-band Bruker system ESP300, equipped with a Bruker ER035 M gaussmeter and a HP 5350B microwave counter. Cyclic voltammetric, differential pulse voltammetric, and coulometric measurements were carried out using a PAR model 273A electrochemistry system. Platinum wire working and auxiliary electrodes and an aqueous saturated calomel reference electrode (SCE) were used in a three-electrode configuration. The supporting electrolyte was Et₄NClO₄, and the solute concentration was ~10⁻³ M. The half-wave potential E°₂₉₈ was set equal to 0.5(E_{pa} + E_{pc}), where E_{pa} and E_{pc} are anodic and cathodic cyclic voltammetric peak potentials, respectively. Elemental analysis was carried out with a Perkin-Elmer 240C elemental analyzer. Electrospray mass spectra were recorded on a Micromass Q-ToF mass spectrometer.

Preparation of Complex {(μ -Nindigo⁰)[Ru(acac)₂]₂} (1). A mixture of Ru(acac)₂(CH₃CN)₂ (100 mg, 0.26 mmol), ligand (L = indigo-N,N'-diphenyldiimine) (53 mg, 0.13 mmol), and Et₃N (24 mg, 0.24 mmol, freshly distilled over KOH) was heated to reflux under atmospheric condition in EtOH for 15 h. The initial orange solution gradually changed to deep blue. The reaction mixture was evaporated to dryness under reduced pressure and purified by column chromatography on neutral alumina. Deep blue 1 was eluted with a mixture of *n*-hexane/CH₂Cl₂ (1:2). Evaporation of the solvent under reduced pressure yielded the pure complex 1 as a dark colored solid, which was further dried under vacuum. Yield: 80 mg (60%). ¹H NMR in CDCl₃ [δ/ppm (J/Hz)]: 8.01 (d, 8.16, 1H), 7.54 (d, 6.52, 1H), 7.49 (t, 6.24, 6.15, 1H), 7.34 (m, 2H), 7.26 (m, 6H), 7.13 (d, 5.24, 2H), 6.96 (t, 7.12, 7.16, 1H), 6.70 (t, 6.12, 6.4, 1H), 6.58 (d, 5.84, 1H), 6.50 (d, 7.88, 1H), 6.09 (d, 7.44, 1H), 5.48 (s, 1H, CH(acac)), 5.22 (s, 1H, CH(acac)), 5.06 (s, 1H, CH(acac)), 5.02 (s, 1H, CH(acac)), 2.23 (s, 3H, CH₃(acac)), 2.14 (s, 3H, CH₃(acac)), 2.13 (s, 3H, CH₃(acac)), 1.93 (s, 3H, CH₃(acac)), 1.85 (s, 3H, CH₃(acac)), 1.83 (s, 3H, CH₃(acac)), 1.79 (s, 3H, CH₃(acac)), 1.75 (s, 3H, CH₃(acac)). MS (ESI⁺, MeCN): *m/z* {[MH]⁺} calcd, 1010.05; found, 1010.41. Molar conductivity (MeCN): Α_M = 6 Ω⁻¹ cm² M⁻¹. Anal. Calcd for C₄₈H₄₀N₄O₈Ru₂: C, 57.13; H, 4.59; N, 5.55. Found: C, 57.43; H, 4.44; N, 5.27.

Crystal Structure Determination. Single crystals were grown by slow evaporation of a solution of 1 in CH₂Cl₂/*n*-hexane (1:1) mixture. X-ray crystal data were collected on a CCD Agilent Technologies (Oxford Diffraction) SUPER NOVA diffractometer. Data collection was evaluated by using the CrysAlisPro CCD software. The data were collected by the standard phi-omega scan techniques, and were scaled and reduced using CrysAlisPro RED software. The structure was solved by direct method using SHELXS-97 and refined by full matrix least-squares with SHELXL-97, refining on F².²¹ All non-hydrogen atoms were refined anisotropically. The remaining hydrogen atoms were placed in geometrically constrained positions and refined with isotropic temperature factors, generally 1.2U_{eq} of their parent atoms. Hydrogen atoms were included in the refinement process as per the riding model. Hydrogen atoms of the solvent water molecules could not be located; however, these have been considered for the empirical formula in Table 6.

Table 6. Selected Crystallographic Data for 1 × 1.5H₂O (*rac*)

compound	1 × 1.5H ₂ O
empirical formula	C ₄₈ H ₄₉ N ₄ O _{9.50} Ru ₂
formula weight	1033.03
crystal system	monoclinic
space group	C2/c
<i>a</i> (Å)	21.5351(4)
<i>b</i> (Å)	13.4540(5)
<i>c</i> (Å)	16.2783(4)
α (deg)	90
β (deg)	92.024(2)
γ (deg)	90
<i>V</i> (Å ³)	4713.4(2)
<i>Z</i>	4
μ (mm ⁻¹)	0.700
<i>T</i> (K)	150(2)
<i>D</i> _{calcd} (g cm ⁻³)	1.456
<i>F</i> (000)	2104
θ range (deg)	3.05–25.00
data/restraints/parameters	4129/0/303
R1, wR2 [<i>I</i> > 2σ(<i>I</i>)]	0.0379, 0.0982
R1, wR2 (all data)	0.0475, 0.1059
GOF	1.065
largest diff. peak/hole (e Å ⁻³)	1.130/−0.588

Computational Details. Full geometry optimizations were carried out by using the density functional theory method at the (R)B3LYP level for 1, 1²⁻ and (U)B3LYP level for 1⁺, 1²⁺, 1³⁺, 1⁻, and 1²⁻ for both the *meso* and the *rac* isomers.²² Except ruthenium, all other elements were assigned the 6-31G* basis set. The LANL2DZ basis set with effective core potential was employed for the ruthenium atom.²³ The vibrational frequency calculations were performed to ensure that the optimized geometries represent the local minima and there are only positive eigenvalues. All calculations were performed with the Gaussian 09 program package.²⁴ Vertical electronic excitations based on (R)B3LYP/(U)B3LYP optimized geometries were computed for 1["] (*n* = +3, +2, +1, 0, 1-, 2-) using the time-dependent density functional theory (TD-DFT) formalism²⁵ in acetonitrile using the conductor-like polarizable continuum model (CPCM).²⁶ GaussSum²⁷ was used to calculate the fractional contributions of various groups to each molecular orbital. All calculated structures were visualized with ChemCraft.

ASSOCIATED CONTENT

S Supporting Information

X-ray crystallographic files in CIF format for *rac*-1, DFT data set for 1["] (Tables S1–S22, Figures S2–S3, S5), mass spectrum

of **1** (Figure S1), and ^1H NMR spectrum of **1** (Figure S4). This material is available free of charge via the Internet at <http://pubs.acs.org>.

AUTHOR INFORMATION

Corresponding Author

*Tel.: +91 22 25767159 (G.K.L.); +49(0)711/685-64170 (W.K.). Fax: +91 22 25723480 (G.K.L.); +49(0)711/685-64165 (W.K.). E-mail: lahiri@chem.iitb.ac.in (G.K.L.); kaim@iac.uni-stuttgart.de (W.K.).

Notes

The authors declare no competing financial interest.

ACKNOWLEDGMENTS

Financial support received from the Department of Science and Technology and the Council of Scientific and Industrial Research (fellowship to P.M. and A.D.), New Delhi (India), the DAAD, FCI, and DFG (Germany) is gratefully acknowledged.

REFERENCES

- (1) Kaim, W. *Inorg. Chem.* **2011**, *50*, 9752–9765.
- (2) (a) Kaim, W.; Lahiri, G. K. *Angew. Chem.* **2007**, *119*, 1808–1828.
(b) Kaim, W.; Lahiri, G. K. *Angew. Chem., Int. Ed.* **2007**, *46*, 1778–1796.
- (3) Ernst, S.; Hänel, P.; Jordanov, J.; Kaim, W.; Kasack, V.; Roth, E. *J. Am. Chem. Soc.* **1989**, *111*, 1733–1738.
- (4) (a) Patra, S.; Sarkar, B.; Maji, S.; Fiedler, J.; Urbanos, F. A.; Jiménez-Aparicio, R.; Kaim, W.; Lahiri, G. K. *Chem.-Eur. J.* **2006**, *12*, 489–498.
(b) Kar, S.; Sarkar, B.; Ghumaan, S.; Janardanan, D.; Slageren, J. V.; Fiedler, J.; Puranik, V. G.; Sunoj, R. B.; Kaim, W.; Lahiri, G. K. *Chem.-Eur. J.* **2005**, *11*, 4901–4911.
(c) Ghumaan, S.; Sarkar, B.; Patra, S.; Parimal, K.; Slageren, J. V.; Fiedler, J.; Kaim, W.; Lahiri, G. K. *Dalton Trans.* **2005**, 706–712.
(d) Kar, S.; Chanda, N.; Mobin, S. M.; Datta, A.; Urbanos, F. A.; Puranik, V. G.; Jiménez-Aparicio, R.; Lahiri, G. K. *Inorg. Chem.* **2004**, *43*, 4911–4920.
(e) Sarkar, B.; Kaim, W.; Klein, A.; Schwederski, B.; Fiedler, J.; Duboc-Toia, C.; Lahiri, G. K. *Inorg. Chem.* **2003**, *42*, 6172–6174.
(f) Chakraborty, S.; Laye, R. H.; Munshi, P.; Paul, R. L.; Ward, M. D.; Lahiri, G. K. *J. Chem. Soc., Dalton Trans.* **2002**, 2348–2353.
(g) Sarkar, B.; Laye, R. H.; Mondal, B.; Chakraborty, S.; Paul, R. L.; Jeffery, J. C.; Puranik, V. G.; Ward, M. D.; Lahiri, G. K. *J. Chem. Soc., Dalton Trans.* **2002**, 2097–2101.
(h) Chakraborty, S.; Laye, R. H.; Paul, R. L.; Gonnade, R. G.; Puranik, V. G.; Ward, M. D.; Lahiri, G. K. *J. Chem. Soc., Dalton Trans.* **2002**, 1172–1179.
- (5) (a) Roy, S.; Sarkar, B.; Imrich, H.-G.; Fiedler, J.; Záliš, S.; Jiménez-Aparicio, R.; Urbanos, F. A.; Mobin, S. M.; Lahiri, G. K.; Kaim, W. *Inorg. Chem.* **2012**, *51*, 9273–9281.
(b) Agarwala, H.; Scherer, T.; Maji, S.; Mondal, T. K.; Mobin, S. M.; Fiedler, J.; Urbanos, F. A.; Jiménez-Aparicio, R.; Kaim, W.; Lahiri, G. K. *Chem.-Eur. J.* **2012**, *18*, 5667–5675.
(c) Das, A.; Scherer, T.; Maji, S.; Mondal, T. K.; Mobin, S. M.; Urbanos, F. A.; Jiménez-Aparicio, R.; Kaim, W.; Lahiri, G. K. *Inorg. Chem.* **2011**, *50*, 7040–7049.
(d) Kumbhakar, D.; Sarkar, B.; Maji, S.; Mobin, S. M.; Fiedler, J.; Urbanos, F. A.; Jiménez-Aparicio, R.; Kaim, W.; Lahiri, G. K. *Chem.-Eur. J.* **2008**, *14*, 10816–10828.
(g) Maji, S.; Sarkar, B.; Mobin, S. M.; Fiedler, J.; Urbanos, F. A.; Jiménez-Aparicio, R.; Kaim, W.; Lahiri, G. K. *Inorg. Chem.* **2008**, *47*, 5204–5211.
(h) Maji, S.; Sarkar, B.; Mobin, S. M.; Fiedler, J.; Urbanos, F. A.; Jiménez-Aparicio, R.; Kaim, W.; Lahiri, G. K. *Dalton Trans.* **2007**, 2411–2418.
(i) Maji, S.; Sarkar, B.; Patra, S.; Fiedler, J.; Mobin, S. M.; Puranik, V. G.; Kaim, W.; Lahiri, G. K. *Inorg. Chem.* **2006**, *45*, 1316–1325.
(j) Sarkar, B.; Patra, S.; Fiedler, J.; Sunoj, R. B.; Janardanan, D.;
- Mobin, S. M.; Niemeyer, M.; Lahiri, G. K.; Kaim, W. *Angew. Chem., Int. Ed.* **2005**, *44*, 5655–5658.
(k) Ghumaan, S.; Sarkar, B.; Patra, S.; Slageren, J. V.; Fiedler, J.; Kaim, W.; Lahiri, G. K. *Inorg. Chem.* **2005**, *44*, 3210–3214.
(l) Patra, S.; Sarkar, B.; Ghumaan, S.; Fiedler, J.; Kaim, W.; Lahiri, G. K. *Inorg. Chem.* **2004**, *43*, 6108–6113.
(m) Patra, S.; Miller, T. A.; Sarkar, B.; Niemeyer, M.; Ward, M. D.; Lahiri, G. K. *Inorg. Chem.* **2003**, *42*, 4707–4713.
- (6) Kaim, W.; Sarkar, B. *Coord. Chem. Rev.* **2007**, *251*, 584–594.
- (7) (a) Nawn, G.; Waldie, K. M.; Oakley, S. R.; Peters, B. D.; Mandel, D.; Patrick, B. O.; McDonald, R.; Hicks, R. G. *Inorg. Chem.* **2011**, *50*, 9826–9837.
(b) Oakley, S. R.; Nawn, G.; Waldie, K. M.; Maclnnis, T. D.; Patrick, B. O.; Hicks, R. G. *Chem. Commun.* **2010**, *46*, 6753–6755.
(c) Nawn, G.; Oakley, S. R.; Majewski, M. B.; MacDonald, R.; Patrick, B. O.; Hicks, R. J. *Chem. Sci.* **2013**, *4*, 612–621.
- (8) Fortier, S.; Moral, O. G.; Chen, C. H.; Pink, M.; Le Roy, J. J.; Murugesu, M.; Mindiola, D. J.; Caulton, K. G. *Chem. Commun.* **2012**, *48*, 11082–11084.
- (9) Kar, S.; Sarkar, B.; Ghumaan, S.; Leboschka, M.; Fiedler, J.; Kaim, W.; Lahiri, G. K. *Dalton Trans.* **2007**, 1934–1938.
- (10) Kaim, W.; Sieger, M.; Greulich, S.; Sarkar, B.; Fiedler, J.; Záliš, S. *J. Organomet. Chem.* **2010**, *695*, 1052–1058.
- (11) Creutz, C. *Prog. Inorg. Chem.* **1983**, *30*, 1–73.
- (12) Kumbhakar, D.; Sarkar, B.; Das, A.; Das, A. K.; Mobin, S. M.; Fiedler, J.; Kaim, W.; Lahiri, G. K. *Dalton Trans.* **2009**, 9645–9652.
- (13) Głowacki, E. D.; Voss, G.; Leonat, L.; Irimia-Vladu, M.; Bauer, S.; Sariciftci, N. S. *Isr. J. Chem.* **2012**, *52*, 540–551.
- (14) Patra, S.; Sarkar, B.; Ghumaan, S.; Fiedler, J.; Záliš, S.; Kaim, W.; Lahiri, G. K. *Dalton Trans.* **2004**, 750–753.
- (15) Poppe, J.; Moschersch, M.; Kaim, W. *Inorg. Chem.* **1993**, *32*, 2640–2643.
- (16) (a) Kaim, W.; Ernst, S.; Kasack, V. *J. Am. Chem. Soc.* **1990**, *112*, 173–178.
(b) Patra, S.; Sarkar, B.; Mobin, S. M.; Kaim, W.; Lahiri, G. K. *Inorg. Chem.* **2003**, *42*, 6469–6473.
(c) Sarkar, B.; Frantz, S.; Roy, S.; Sieger, M.; Duboc, C.; Denninger, G.; Kümmeler, H. J.; Kaim, W. *J. Mol. Struct.* **2008**, *890*, 133–138.
- (17) (a) Kar, S.; Sarkar, B.; Ghumaan, S.; Roy, D.; Urbanos, F. A.; Fiedler, J.; Sunoj, R. B.; Jiménez-Aparicio, R.; Kaim, W.; Lahiri, G. K. *Inorg. Chem.* **2005**, *44*, 8715–8722.
(b) Hoshino, Y.; Higuchi, S.; Fiedler, J.; Su, C. Y.; Knödler, A.; Schwederski, B.; Sarkar, B.; Hartmann, H.; Kaim, W. *Angew. Chem.* **2003**, *115*, 698–701.
(c) Hoshino, Y.; Higuchi, S.; Fiedler, J.; Su, C. Y.; Knödler, A.; Schwederski, B.; Sarkar, B.; Hartmann, H.; Kaim, W. *Angew. Chem., Int. Ed.* **2003**, *42*, 674–677.
- (18) Robin, M. B.; Day, P. *Adv. Inorg. Chem. Radiochem.* **1967**, *10*, 247–422.
- (19) Kobayashi, T.; Nishina, Y.; Shinizu, K. G.; Satô, G. P. *Chem. Lett.* **1988**, 1137–1140.
- (20) Krejcik, M.; Danek, M.; Hartl, F. *J. Electroanal. Chem.* **1991**, *317*, 179–187.
- (21) (a) Sheldrick, G. M. *Acta Crystallogr., Sect. A* **2008**, *A64*, 112–122.
(b) *Program for Crystal Structure Solution and Refinement*; University of Goettingen: Goettingen, Germany, 1997.
- (22) Lee, C.; Yang, W.; Parr, R. G. *Phys. Rev. B* **1988**, *37*, 785–789.
- (23) (a) Andrae, D.; Haessermann, U.; Dolg, M.; Stoll, H.; Preuss, H. *Theor. Chim. Acta* **1990**, *77*, 123–141.
(b) Fuentealba, P.; Preuss, H.; Stoll, H.; Szenthpaly, L. V. *Chem. Phys. Lett.* **1989**, *89*, 418–422.
- (24) Frisch, M. J.; Trucks, G. W.; Schlegel, H. B.; Scuseria, G. E.; Robb, M. A.; Cheeseman, J. R.; Scalmani, G.; Barone, V.; Mennucci, B.; Petersson, G. A.; Nakatsuji, H.; Caricato, M.; Li, X.; Hratchian, H. P.; Izmaylov, A. F.; Bloino, J.; Zheng, G.; Sonnenberg, J. L.; Hada, M.; Ehara, M.; Toyota, K.; Fukuda, R.; Hasegawa, J.; Ishida, M.; Nakajima, T.; Honda, Y.; Kitao, O.; Nakai, H.; Vreven, T.; Montgomery, J. A., Jr.; Peralta, J. E.; Ogliaro, F.; Bearpark, M.; Heyd, J. J.; Brothers, E.; Kudin, K. N.; Staroverov, V. N.; Kobayashi, R.; Normand, J.; Raghavachari, K.; Rendell, A.; Burant, J. C.; Iyengar, S. S.; Tomasi, J.; Cossi, M.; Rega, N.; Millam, J. M.; Klene, M.; Knox, J. E.; Cross, J. B.; Bakken, V.; Adamo, C.; Jaramillo, J.; Gomperts, R.; Stratmann, R. E.; Yazayev, O.; Austin, A. J.; Cammi, R.; Pomelli, C.; Ochterski, J. W.; Martin, R. L.; Morokuma, K.; Zakrzewski, V. G.; Voth, G. A.; Salvador, P.;

Dannenberg, J. J.; Dapprich, S.; Daniels, A. D.; Farkas, O.; Foresman, J. B.; Ortiz, J. V.; Cioslowski, J.; Fox, D. J. *Gaussian 09*, revision A.02; Gaussian, Inc.: Wallingford, CT, 2009.

(25) (a) Bauernschmitt, R.; Ahlrichs, R. *Chem. Phys. Lett.* **1996**, *256*, 454–464. (b) Stratmann, R. E.; Scuseria, G. E.; Frisch, M. J. *J. Chem. Phys.* **1998**, *109*, 8218–8225. (c) Casida, M. E.; Jamorski, C.; Casida, K. C.; Salahub, D. R. *J. Chem. Phys.* **1998**, *108*, 4439–4450.

(26) (a) Barone, V.; Cossi, M. *J. Phys. Chem. A* **1998**, *102*, 1995–2001. (b) Cossi, M.; Barone, V. *J. Chem. Phys.* **2001**, *115*, 4708–4718. (c) Cossi, M.; Rega, N.; Scalmani, G.; Barone, V. *J. Comput. Chem.* **2003**, *24*, 669–681.

(27) O'Boyle, N. M.; Tenderholt, A. L.; Langner, K. M. *J. Comput. Chem.* **2008**, *29*, 839–845.